

Verification of a Remaining Flying Time Prediction System for Small Electric Aircraft

Edward F. Hogge¹, Brian M. Bole², Sixto L. Vazquez³, José R. Celaya⁴, Thomas H. Strom⁵, Boyd L. Hill⁶, Kyle M. Smalling⁷, and Cuong C. Quach⁸

^{1,5,7}*Northrop Grumman Technical Services, NASA Langley Research Center, Hampton, Virginia 23681*

edward.f.hogge@nasa.gov

thomas.h.strom@nasa.gov

kyle.m.smalling@nasa.gov

^{2,4}*Stinger Ghaffarian Technologies, Inc., NASA Ames Research Center, Moffett Field, California 94035*

brian.m.bole@nasa.gov

jose.r.celaya@nasa.gov

^{3,8}*NASA Langley Research Center, Hampton, Virginia 23681*

sixto.l.vazquez@nasa.gov

cuong.c.quach@nasa.gov

⁶*Analytical Mechanics Associates, Inc., NASA Langley Research Center, Hampton, Virginia 23681*

boyd.l.hill@nasa.gov

ABSTRACT

This paper addresses the problem of building trust in online predictions of a battery powered aircraft's remaining available flying time. A set of ground tests is described that make use of a small unmanned aerial vehicle to verify the performance of remaining flying time predictions. The algorithm verification procedure described here uses a fully functional vehicle that is restrained to a platform for repeated run-to-functional-failure experiments. The vehicle under test is commanded to follow a predefined propeller RPM profile in order to create battery demand profiles similar to those expected in flight. The fully integrated aircraft is repeatedly operated until the charge stored in powertrain batteries falls below a specified lower-limit. The time at which the lower-limit on battery charge is crossed is then used to measure the accuracy of remaining flying time predictions. Accuracy requirements are considered in this paper for an alarm that warns operators when remaining flying time is estimated to fall below a specified threshold.

1. INTRODUCTION

Improvements in battery storage capacity have made it possible for general aviation vehicle manufacturers to

consider electrically-powered solutions. The development of trust in battery remaining operating time estimates, however, is currently a significant obstacle to be overcome when considering adoption of electrical propulsion systems in aircraft (Patterson, German & Moore, 2012). There are several ways in which predicting remaining operating time is more complicated for battery-powered vehicles than it is for vehicles with a conventionally-powered liquid-fueled combustion system. Unlike a liquid-fueled system, where the fuel tank's volume remains unchanged over successive refueling procedures, a battery's charge storage capacity will diminish over time. Another complicating feature of a battery system is the time-varying relationship between battery output power and battery current draw. Whereas a conventional liquid combustion system uses an approximately constant amount of liquid fuel to produce a given motive power, the power from a battery system is equal to the product of battery voltage and current. Thus, as batteries are discharged, their voltages drop lower, and they will lose charge at a faster rate.

Our previous papers introduced several new tools for battery discharge prediction onboard a small electric aircraft. One paper described a battery equivalent circuit model to simulate battery state (Bole, Teubert, Quach, Hogge, Vazquez & Goebel, 2013). The model's battery capacity, internal resistance and other parameters were identified through two laboratory experiments that used a programmed load. The batteries were slowly discharged in one experiment. In the other experiment a repeated pulsed loading was done. Current

Edward Hogge et al. This is an open-access article distributed under the terms of the Creative Commons Attribution 3.0 United States License, which permits unrestricted use, distribution, and reproduction in any medium, provided the original author and source are credited.

and voltage profiles logged during flights of a small electric airplane further tuned the battery model (Quach, Bole, Hogge, Vazquez, Daigle, Celaya, Weber & Goebel, 2013). The use of a flight plan with upper and lower uncertainty bounds on the required energy to complete the mission successfully was presented along with an approach to identify additional parasitic battery loads (Bole, Daigle & Gorospe, 2014). This paper introduces a verification testing procedure that is intended to build trust in predictions of remaining flying time prior to actual flight testing. The philosophy behind the testing procedure described here is to translate system performance and safety goals into requirements for an alarm that warns system operators when the estimated remaining flying time falls below a certain threshold. Ground testing of the actual vehicle provides the closest possible testing conditions short of actual flight and captures some of the variation that the powertrain hardware and that the pilot may introduce while avoiding the risks inherent in flight. For instance, the batteries may be drained to a lower capacity during testing of the remaining flying time prediction without danger of vehicle loss.

A small electric unmanned aerial vehicle (e-UAV) was used in this study. The e-UAV is a 33% sub-scale version of the Zivko Aeronautics Inc. Edge 540 T tandem seat aerobatic aircraft. This vehicle has been actively used by researchers at NASA LaRC to facilitate the rapid deployment and evaluation of remaining flying time prediction algorithms for electric aircraft since 2010. Examples of prior works using this platform are found in the following papers: (Saha, Koshimoto, Quach, Hogge, Strom, Hill, Vazquez & Goebel, 2011), (Hogge, Quach, Vazquez & Hill, 2011), (Daigle, Saxena & Goebel, 2012), and (Bole et al., 2013).

Remaining flying time prediction algorithms focus on the prediction of battery charge depletion over an e-UAV flight. A lower-bound on the battery state of charge (SOC) that is considered safe for flight is set at 30% in this work. Flying the vehicle with batteries below 30% SOC is considered to be a high-risk mode of operation that violates the vehicle's safe operating guidelines. Such violations of operating guidelines are referred to here as a functional failure of the vehicle's mission.

The accuracy of onboard remaining flying time estimation algorithms is tested in this work, by conducting a series of controlled run-to-functional-failure experiments on the ground. The vehicle under test was strapped down to a platform and commanded to follow an RPM profile that creates battery demand profiles similar to those expected for flight. A picture of the e-UAV strapped down for ground-based testing is shown in Fig. 1.

The time it takes for powertrain batteries to reach 30% SOC establishes a truth value for the functional failure time. Unlike actual flight tests, powertrain batteries can be repeatedly run down to their lower-limits in the ground-based



Figure 1. The Edge 540 T Rapid Evaluation e-UAV

testing described here to verify the accuracy of remaining flying time predictions.

The primary use-case for remaining flying time predictions is to warn system operators when landing procedures must be initiated to avoid aircraft batteries falling below 30% SOC. After consulting with system operators, it was determined that initiating landing procedures at least two minutes before e-UAV batteries would reach 30% SOC under normal operations provided a sufficient energy buffer for landing maneuvers. The predictive element to be tested in this work is an alarm that warns system operators when the powertrain batteries are two minutes from reaching 30% SOC under normal operations.

System operators were also consulted to identify performance requirements on the prognostic alarm. The defined performance requirements were then verified by repeating ground-based run-to-functional-failure tests a specified number of times. The performance requirement testing procedure explained here was originally introduced in (Saxena, Roychoudhury, Lin & Goebel, 2013).

Section 2 of this paper provides an overview of the Edge 540T powertrain. Algorithms used for onboard battery state estimation and remaining flying time predictions are summarized in Section 3. The process used to verify onboard remaining flying time predictions through ground testing and experimental results are described in Section 4. Finally, concluding remarks are given in Section 5.

2. OVERVIEW OF EDGE 540T POWERTRAIN

A wiring diagram for the vehicle powertrain is shown in Fig. 2. The aircraft has two 3-phase tandem motors that are mechanically coupled to the aircraft propeller. Powertrain batteries are arranged in two pairs of series connected battery packs. A switchable parasitic load R_p is present to test the robustness of remaining flying time estimation algorithms to changes in battery loading demands. The other symbols in the figure identify the location of current and voltage sensors.

Remaining flying time predictions are generated by propagating present battery charge estimates forward. Forward propagation of present battery state estimates is

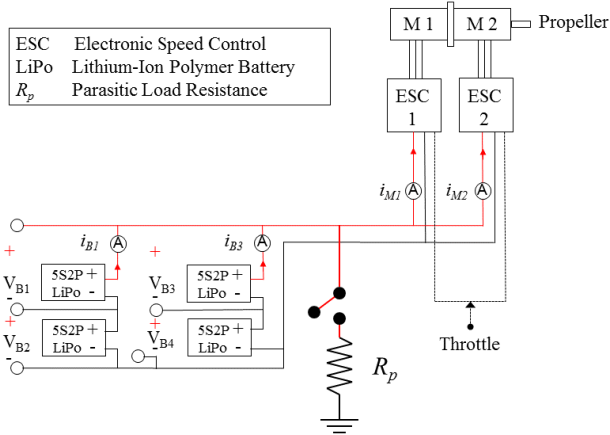


Figure 2. Schematic of electric Powertrain.

performed using estimates of future powertrain demands that will occur over a known flight plan. These future loads include propeller loads and parasitic loads. The prognostic tools used in this work make use of a known flight plan to inform future load predictions, but no prior information is assumed to be available regarding when a parasitic load may be injected.

3. REMAINING FLYING TIME PREDICTION

Battery discharge prediction is described here in terms of the following components; (i) online battery state estimation; (ii) prediction of future battery power demand as a function of an aircraft flight plan; (iii) online estimation of additional parasitic battery loads; and (iv) prediction of battery discharge over the future flight plan. The assumptions and algorithms used for each of these steps are summarized in this section.

3.1. Online Battery State Estimation

Our previous papers (Quach et al., 2013) and (Bole et al., 2014), described the use of an equivalent circuit model and unscented Kalman filtering (UKF) to update battery state estimates based on observations of current and voltage at the battery output terminals. This approach is also summarized here for convenience. Figure 3 shows an equivalent circuit battery model that is used to represent battery output voltage dynamics as a function of battery current. This battery model contains six electrical components that are tuned to recreate the observed current-voltage dynamics of the Edge-540T battery packs. The bulk of battery charge is assumed to be stored in the capacitor, C_b . The (R_s, C_s) and (R_{cp}, C_{cp}) circuit element pairs are used to simulate standard battery phenomenon, such as internal resistance drops and hysteresis effects. Additionally, because battery input-output dynamics will change as a function of internal battery charge, it is necessary to parameterize some of the circuit components in

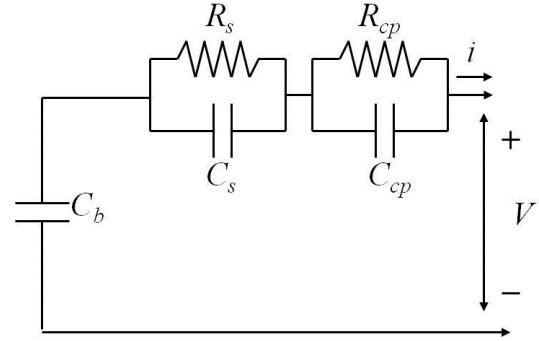


Figure 3. Lithium-Ion battery equivalent circuit model

terms of the bulk charge stored in C_b as described in (Zhang and Chow, 2010).

The UKF takes in the measured battery current and voltage, and gives probability distributions for the charge states of each of the three capacitors in the equivalent circuit model as output. Implementation details for the equivalent circuit model and UKF state estimation are omitted here. Readers interested in the application of UKF to the estimation of battery SOC are referred to our previous paper, (Bole et al., 2014). It is sufficient to state here that the equivalent circuit battery model and the UKF state estimation routine are assumed to do an adequate job of tracking the total charge within the battery over an arbitrary usage profile.

The ratio of a battery's current charge to its maximum charge storage capacity is typically referred to as the state of charge (SOC). Battery SOC is defined here as:

$$SOC = 1 - \frac{q_{max} - q_b}{C_{max}} \quad (1)$$

where q_b represents the charge stored in capacitor C_b , q_{max} is the maximum charge that the battery can hold, and C_{max} is the maximum charge that can be drawn from the battery in practice. Here, C_{max} will always be less than q_{max} , due to electrochemical side-reactions that make some portion of a battery's charge carriers unavailable. As the battery ages more of its internal charge will become unavailable because of these side reactions. The C_{max} parameter must be refitted periodically to capture this effect.

3.2. Prediction of Motor Power Demand as a Function of Aircraft Flight Plan

After estimating battery state, the next step towards predicting remaining flying time is the estimation of motor power demand over the remainder of a given flight plan. The aircraft's flight plan is assumed here to be specified in advance in terms of a fixed set of segments. Each segment includes a desired vehicle airspeed along with an expected duration or other ending condition. An example flight plan is defined here as:

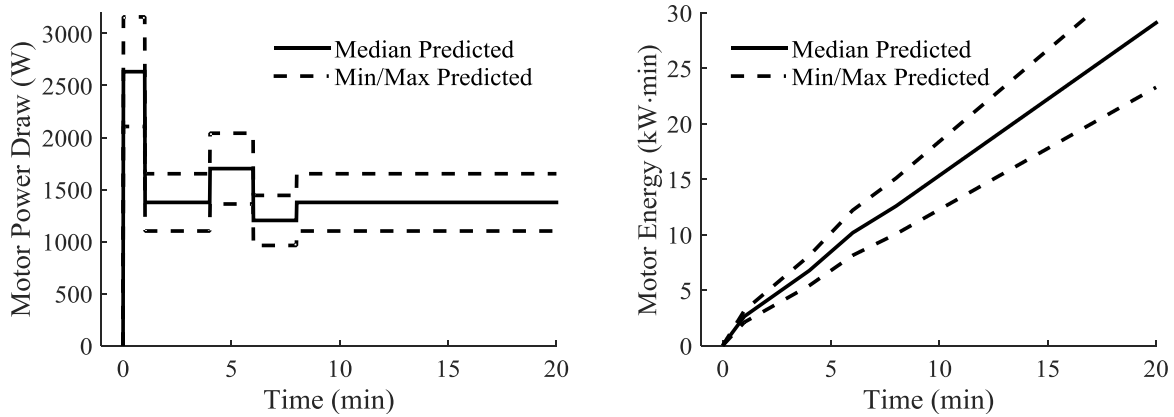


Figure 4. Uncertain predictions of motor power and energy draw over the sample flight plan

1. **Takeoff and climb to 200 m:** desired airspeed = 20 m/s, duration = 1.0 min
2. **Maintain altitude, airspeed set point:** desired airspeed = 23 m/s, duration = 3.0 min
3. **Maintain altitude, increase airspeed set point:** desired airspeed = 25 m/s, duration = 2.0 min
4. **Maintain altitude, decrease airspeed set point:** desired airspeed = 18 m/s, duration = 2.0 min
5. **Maintain altitude, increase airspeed set point:** desired airspeed = 23 m/s, duration = fly until landing is called by monitors on the ground.
6. **Remote control landing:** airspeed and duration may vary widely depending on pilot and environmental conditions.

It is important to understand the granularity at which the flight plan is specified. Note that this flight plan specifies desired speed set points, but does not specify a rate at which the vehicle must switch from one speed to another. Also note that while the flight plan specifies a desired speed, it does not specify exactly how close the aircraft must be to the desired speed. These details are left open to the interpretation of the pilot or autopilot.

The energy needed for an aircraft to fly the remainder of a given flight plan will necessarily be uncertain due to random variation in pilot behavior and environmental conditions. A minimum, maximum, and median motor power demand for each remaining segment of the flight plan is used in this work to represent prediction uncertainty. These three power estimates can then be integrated to form predictions of the minimum, maximum, and median motor energy consumption over the remaining flight plan.

Figure 4 shows sample predictions of future motor power and energy demand over segments 1-5 of the given flight plan. Here, segment 5 of the flight plan is shown to extend out indefinitely, representing the intent to continue flying until the ground team calls for a landing. The median motor power

demands are estimated for each flight plan segment using a previously developed model, discussed in Bole et al. (2013) and Bole et al. (2014). A plus or minus 30% error margin around the median motor power demand estimate was used to generate the minimum and maximum predictions shown in Figure 4.

A constraint on the minimum battery SOC required for safely landing the aircraft is considered to limit the aircraft's maximum safe flying time. This minimum SOC threshold is considered here to be 30%. Prediction of available flying time remaining can thus be considered in this example as the time until the battery SOC reaches 30%, assuming that a landing will not be called until the last possible moment. A triplet of minimum, maximum, and median remaining flying time estimates will ultimately be produced by estimating when the battery SOC threshold would be reached for each of the minimum, maximum, and median motor power profiles.

3.3. Online Estimation of Additional Parasitic Battery Loads

Parasitic demands on the battery system that cannot be known in advance are simulated with a resistive load that may be injected in parallel with the aircraft batteries at any time during flight. This parasitic load is denoted as R_p in Fig. 2. The magnitude of the parasitic load is assumed to be unknown. An online filtering routine, described in Bole et al. (2014), was shown to rapidly converge on estimates of parasitic load using data from the current and voltage sensors shown in Fig. 2. A battery current profile and parasitic load estimates from a sample aircraft data set is shown in Fig. 5. Here, a 5.5 Ω parasitic load is injected in parallel with the aircraft batteries at 5 minutes into the run. The time at which the parasitic load is injected is shown with a dashed line on the third column of plots in Fig. 6. At the time the load is injected the battery current is seen to become notably higher

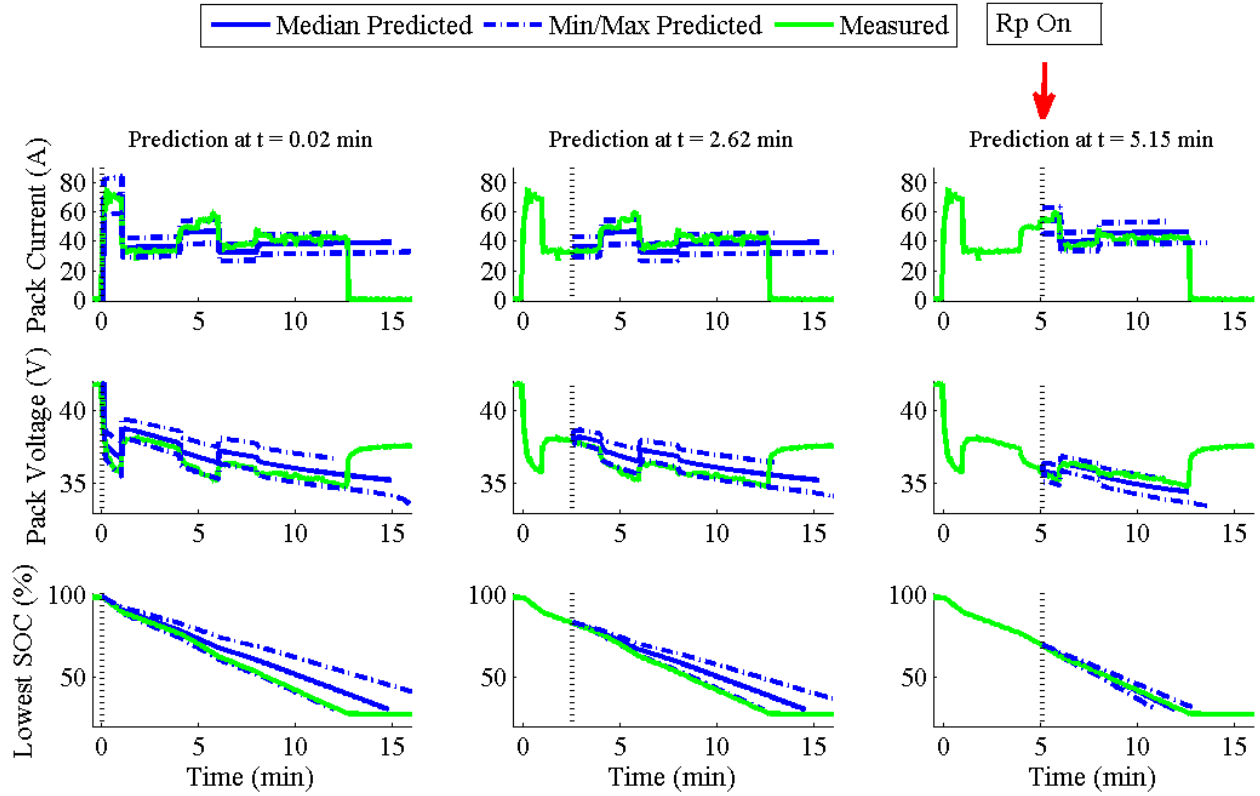


Figure 6. Example plot of measured and predicted battery current (top) and voltage (bottom) shown at three sample times over a trial battery discharge run

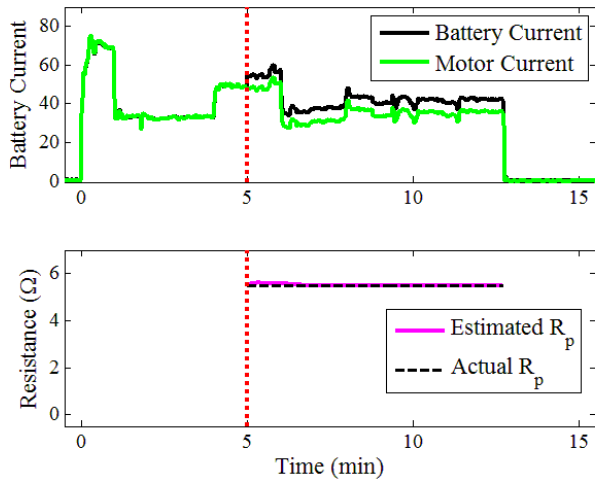


Figure 5. Sample motor and battery current profiles (top), along with parasitic load estimates (bottom)

than the motor current. The estimated parasitic load is then seen to rapidly converge to approximately 5.5Ω .

Online parasitic load estimates are directly incorporated into battery discharge predictions. This results in an immediate shift in battery discharge predictions each time the parasitic

load estimate is updated. This immediate shift in discharge predictions is demonstrated in the following subsection.

3.4. Predicting of Battery Discharge Over a Flight Plan

Figure 6 shows plots of measured and predicted battery current, voltage, and SOC at three sample times over the battery discharge run. The minimum, median, and maximum predictions are plotted from each sample time until the predicted SOC reaches 30%.

The predictions made at the first two sample times occur prior to parasitic load injection. These predictions are seen to under-estimate the future battery current loads, resulting in over-estimates of future battery voltage and SOC. The parasitic load has been detected by the third sample time, and the predictions at that time are seen to be much more closely centered on the measured evolutions of battery current, voltage, and SOC.

Figure 7 shows predictions of remaining flying time for the example run shown in Fig. 6. The dashed line in Fig. 7 indicates the true flying time remaining. The solid line in Fig. 7 represents the median remaining time prediction. The bars in Fig. 7 represent the interval between the minimum and maximum remaining time prediction. Here, the true flying time remaining is found by subtracting the current time from

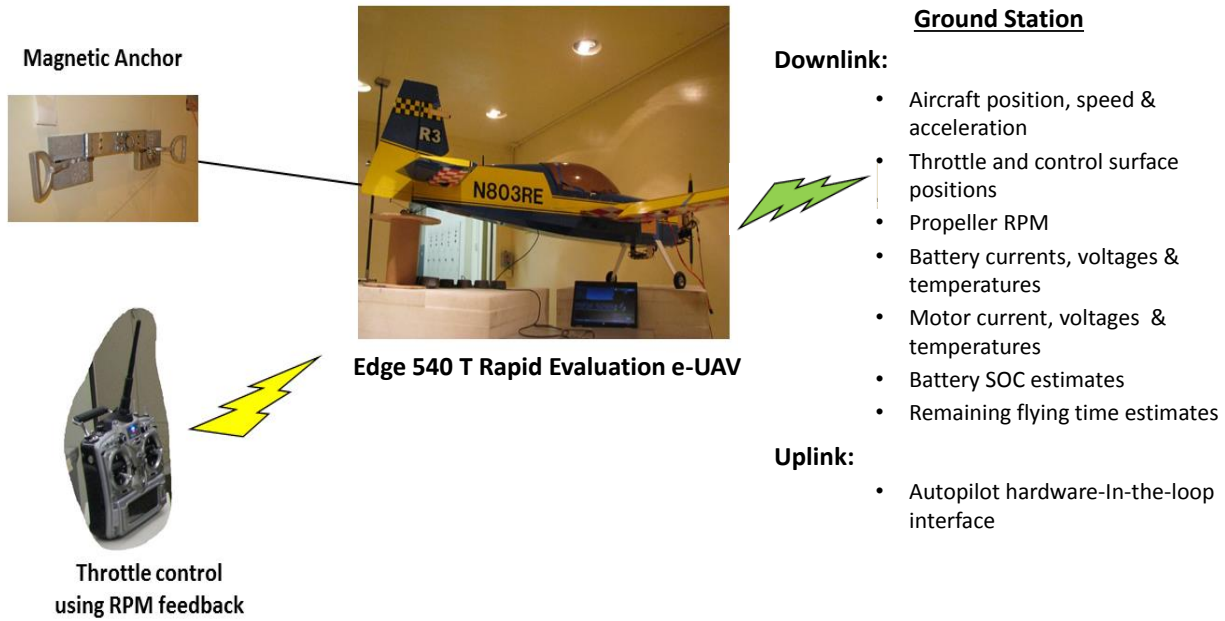


Figure 8. Ground test chamber setup for active motor simulated flight

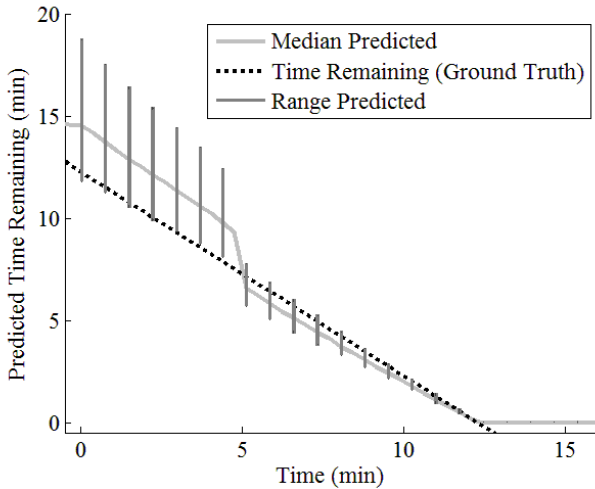


Figure 7. Predicted remaining flying time

the time at which the lowest battery SOC crossed 30%. The predictions are seen to overestimate remaining flying time until the parasitic load is detected at about 5 minutes into the run. After the parasitic load is detected the remaining flying time predictions are immediately shifted down.

4. GROUND TEST VERIFICATION OF REMAINING FLYING TIME PREDICTION

The ground-based verification testing of Edge 540 T hardware and software was performed by strapping the vehicle down in the LaRC Electromagnetics and Sensors

Branch High Intensity Radiated Fields (HIRF) test chamber. More information about the HIRF Chamber can be found in a report of an earlier UAS radio frequency emissions test in (Ely, Koppen, Nguyen, Dudley, Szatkowski, Quach, Vazquez, Mielnik, Hogge, Hill & Strom, 2011). The airplane was placed upon expanded-polystyrene blocks centered within the chamber, as seen in Fig. 8. The aircraft powertrain with propeller was operated with the vehicle anchored using a steel cable to the chamber wall. Its motor and actuators were operated from another room using the same remote control radio that will be used in flight tests.

Measured aircraft states, battery SOC estimates, and remaining flying time estimates were broadcast to a ground station over a wireless downlink. The ground station also had an uplink interface that enables the aircraft's autopilot to autonomously follow a given flight plan in chamber testing. This autopilot hardware-in-the-loop interfacing capability is discussed in (Bole et. al., 2013).

Only manual control was used for the test results described in this paper, although the autopilot interface is expected to be used in future work. Aircraft propeller RPM, estimated battery SOC, and predicted flying time remaining were displayed to system operators by the ground station in near real-time. The motor throttle was commanded using the control radio by a manual operator, who read the RPM display from the ground station. The operator adjusted the remote control throttle to maintain the target values for the time duration as determined by the flight plan described in Section 3.2. The test proceeded until a 28% SOC condition was indicated on the ground station display for the lowest

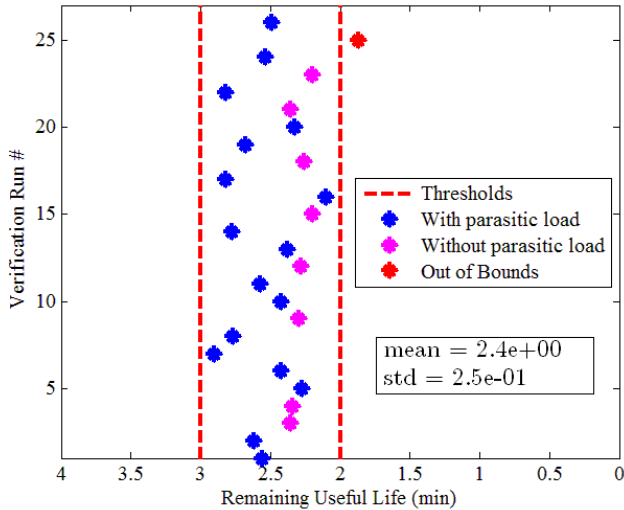


Figure 9. Two-minute alarms for 26 runs

battery. Battery current draw was then stopped and powertrain batteries were allowed to rest for approximately one hour. The battery terminal voltages at rest were used to compute an empirical approximation of ending battery SOC.

Onboard data logging during the experiment runs was performed by the data system described in (Hogge, 2011).

4.1. Performance Requirements

The specification of performance requirements for ground verification of remaining flying time predictions is described next. The predictive element to be tested in this work is an alarm that warns system operators when the powertrain batteries are two minutes from reaching 30% SOC under normal operations.

Accuracy requirements for the two minute warning were specified as:

- *The prognostic algorithm shall raise an alarm no later than two minutes before the lowest battery SOC estimate falls below 30% for at least 90% of verification trial runs.*
- *The prognostic algorithm shall raise an alarm no earlier than three minutes before the lowest battery SOC estimate falls below 30% for at least 90% of verification trial runs.*
- *Verification trial statistics must be computed using at least 20 experimental runs*

Here, the two minute alarm is biased to occur early rather than late since the landing becomes unsafe if not enough fuel reserve is present. The early alarm prediction bound limits the “opportunity cost” of unnecessarily denied flying time.

The requirement definitions above use the term “SOC estimate”, because the UKF state estimation algorithm, described earlier, is relied upon to provide online estimates of battery SOC from measured battery current and voltages. A more direct measurement of battery SOC can be obtained after the experimental run is complete by allowing batteries to rest until the terminal voltage settles to a constant value. There is a known relationship between resting battery voltage and SOC that can then be used to compute the ending SOC of all powertrain batteries. The difference between the estimated battery SOC at the end of each experimental run and the measurement of SOC that is computed from the resting battery voltage is referred to here as the ending SOC estimation error.

An additional requirement for remaining flying time verification testing specifies maximum bounds on the ending SOC estimation error:

The ending SOC estimation error as identified from the resting battery voltage must be less than 5% for at least 90% of verification trial runs.

4.2. Experimental Results

Figure 9 shows the difference between the time at which the two minutes remaining alarm was raised and the time at which the lowest battery SOC estimate crosses 30% for 26 verification runs. Runs that were performed with and without parasitic load injection are identified in the figure. The vertical lines in the figure indicate the bounds on acceptable alarm accuracy. Only one verification run out of the 26 performed is seen to violate the desired accuracy bounds. The requirement that 90% of trials pass this benchmark is thus seen to be satisfied.

Figure 10 shows box plots of the SOC estimation error measured over the 26 verification runs performed. Because each verification run requires 4 powertrain batteries, 104 measurements of SOC estimation error are produced. Only one of these measurements falls outside of the 5% error tolerance allowed. The requirement that 90% of trials pass this benchmark is thus seen to be satisfied.

5. CONCLUSION

A procedure for verifying the performance of remaining flying time predictions for a small electric aircraft was demonstrated. Aircraft battery packs reaching 30% SOC in flight was defined as high risk operation for our experimental flying vehicle, to be avoided if possible. Ground-based simulated flight testing was shown to enable a safe means of running the aircraft power train to 30% SOC in order to obtain an empirical measurement of the aircraft’s available safe operating time.

Ground-based testing enables repeatable run-to-functional-failure testing of remaining flying time predictions using the integrated flight vehicle. Repeatable testing such as that

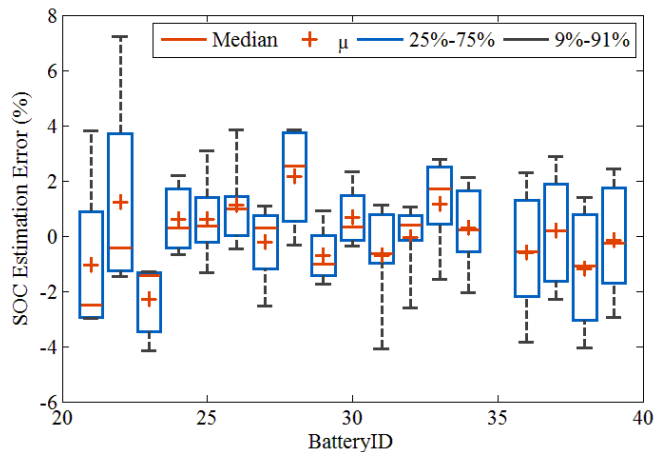


Figure 10. Box plots of the SOC estimation error measured over 26 verification runs that each use 4 batteries

described in this paper is necessary to effectively debug, tune, and build trust in prognostic algorithms prior to deployment in mission critical applications.

ACKNOWLEDGEMENT

This work was funded by the NASA System-wide Safety Assurance Technologies (SSAT) project under the Aviation Safety (AvSafe) Program of the Aeronautics Research Mission Directorate (ARMD), Prognostics and Decision Making. E. Hogge author thanks Mr. Patrick Tae for his contribution to the testing of the parasitic load apparatus as part of his intern assignment.

REFERENCES

- Bole, B., Daigle, M., Gorospe, G., (2014). "Online Prediction of Battery Discharge and Estimation of Parasitic Loads for an Electric Aircraft". *European Conference of the Prognostics and Health Management Society*.
- Bole, B., Teubert, C., Quach, C., Hogge, E., Vazquez, S., Goebel, K., & Vachtsevanos, G. (2013). "SIL/HIL Replication of Electric Aircraft Powertrain Dynamics and Inner-Loop Control for V&V of System Health Management Routines". *Annual Conference of the Prognostics and Health Management Society*.
- Daigle, M., Saxena A. & Goebel, K. (2012). "An Efficient Deterministic Approach to Model-based Prediction Uncertainty Estimation". *Annual Conference of the Prognostics and Health Management Society, 2012*.
- Ely, J., Koppen, S., Nguyen, T., Dudley, K., Szatkowski, G., Quach, C., Vazquez, S., Mielnik, J., Hogge, E., Hill, B. & Strom, T. (2011). "Radiated Emissions From a Remote-Controlled Airplane - Measured in a Reverberation Chamber". NASA/TM-2011-217146.

- Hogge, E., Quach, C., Vazquez, S. & Hill, B. (2011). "A Data System for a Rapid Evaluation Class of Subscale Aerial Vehicle". NASA/TM-2011-217145.
- Quach, C., Bole, B., Hogge, E., Vazquez, S., Daigle, M., Celaya, J., Weber, A. & Goebel, K. (2013). "Battery Charge Depletion Prediction on an Electric Aircraft". *Annual Conference of the Prognostics and Health Management Society 2013*.
- Patterson, N., German, B. J. & Moore, M. D. (2012). "Performance Analysis and Design of On-Demand Electric Aircraft Concepts". *12th AIAA Aviation Technology, Integration, and Operations (ATIO) Conference and 14th AIAA/ISSM* (p. 27). Reston, VA: AIAA.
- Saha, B., Koshimoto, E., Quach, C., Hogge, E., Strom, T., Hill, B., Vasquez, S. & Goebel, K. (2011). "Battery Health Management System for Electric UAV's". *IEEE Aerospace Conference*. Big Sky, MT: IEEE.
- Saha, B., Quach, C., Goebel, K. (2012). "Optimizing Battery Life for Electric UAVs Using a Bayesian Framework". *Aerospace Conference, 2012 IEEE*. Big Sky, MT: IEEE.
- Saxena, A., Roychoudhury, I., Celaya, J., Saha, B., Saha, S. & Goebel, K. (2012). "Requirements Flowdown for Prognostics and Health Management". *Infotech@Aerospace Conference* (pp. 8-9). Garden Grove, CA: AIAA, Reston, VA.
- Saxena, A., Roychoudhury, I., Lin, W. & Goebel, K. (2013). "Towards Requirements in Systems Engineering for Aerospace IVHM Design". *AIAA Conference, 2013*. AIAA, Reston, VA.
- Zhang, H. & Chow, M.-Y. (2010). "Comprehensive dynamic battery modeling for PHEV applications". *Power and Energy Society General Meeting, 2010, IEEE*. Minneapolis, MN: IEEE.

BIOGRAPHIES



Edward F. Hogge received a B.S. in Physics from the College of William and Mary in 1977. He has provided engineering services to the government and currently is employed by Northrop Grumman Technical Services. He has recently been supporting aviation safety research through the implementation of electronic systems for subscale remotely piloted aircraft and through commercial aircraft simulation. He is a member of the American Institute of Aeronautics and Astronautics.



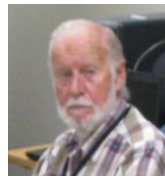
Brian M. Bole graduated from the FSU-FAMU School of Engineering in 2008 with a B.S. in Electrical and Computer Engineering and a B.S. in Applied Math. He received M.S. and Ph.D. degrees in Electrical Engineering from the Georgia Institute of Technology. His research interests include:

analysis of stochastic processes, risk analysis, and optimization of stochastic systems. He is currently investigating the use of risk management and stochastic optimization techniques for prognostics and prognostics-informed decision making in robotic and aviation applications. From 2011 to 2013 he performed joint research with the Prognostic Center of Excellence at NASA Ames under the NASA graduate student research fellowship.



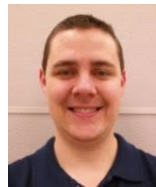
Sixto L. Vazquez Mr. Vazquez obtained MSEE from Old Dominion University in 1990 and BSEE from the University of Puerto Rico in 1983. He has developed real-time 3D graphical simulations to aid in the visualization and analysis of complex sensory data. He has developed techniques

to interactively process, analyze, and integrate sensory data from multiple complex, state-of-the-art sensing technologies, i.e. FMCW Coherent Laser Radar range measuring system, Bragg grating Fiber Optic Strain Sensing system, etc., into simulation. In recent years, he has developed software for the Ardupilot and associated ground station.



Thomas H. Strom was born in Aberdeen, WA, 1924. He graduated from Hoquiam High School in 1942, and attended Seattle University and the University of Washington 1953-1960. He served in the U.S. Navy during World War II as a Radar

Technician. He was an employee of the Boeing Corp. Wind Tunnel, Seattle, WA 1947-1972. He was Senior Engineer with principal expertise in flutter and aeroelastic wind tunnel modeling. He was the founder and president of Dynamic Engineering, Inc., Newport News, VA, until 1997. He has served as a consultant to the Aeroelasticity Group of NASA Langley Research Center (LaRC) and continues to provide engineering and technical services to LaRC through Northrop Grumman Technical Services.



Kyle M. Smalling Kyle Smalling obtained his B.S. in Aerospace Engineering from Cal Poly Pomona in 2013. He is an avid remote control vehicle enthusiast both personally and professionally. His areas of research include Health Prognostics and developing Safety Critical hardware and software. He is

employed by Northrop Grumman Technical Services.



Cuong C. Quach received his M.S. from the School of Physics and Computer Sciences at Christopher Newport University in 1997. He is a staff researcher in the Safety Critical Avionics Systems Branch at NASA Langley Research Center. His research areas include development and testing of software for airframe diagnosis and strategic flight path conflict detection.